

Towards Physically Consistent Deep Learning For Climate Model Parameterizations

Birgit Kühbacher^{a, b, *}, Fernando Iglesias-Suarez^a, Niki Kilbertus^{b, c, d} and Veronika Eyring^{a, c, e}

^aDeutsches Zentrum für Luft- und Raumfahrt (DLR), Institut für Physik der Atmosphäre, Oberpfaffenhofen, Germany

^bHelmholtz Munich, Munich, Germany

^cTechnical University of Munich, Munich, Germany

^dMunich Center for Machine Learning (MCML), Munich, Germany

^eUniversity of Bremen, Institute of Environmental Physics, Bremen, Germany

ORCID (Birgit Kühbacher): <https://orcid.org/0009-0003-6445-8344>

Abstract. Climate models play a critical role in understanding and projecting climate change. Due to their complexity, their horizontal resolution of ~40-100 km remains too coarse to resolve processes such as clouds and convection, which need to be approximated via parameterizations. These parameterizations are a major source of systematic errors and large uncertainties in climate projections. Deep learning (DL)-based parameterizations, trained on computationally expensive, short high-resolution simulations, have shown great promise for improving climate models in that regard. However, their lack of interpretability and tendency to learn spurious non-physical correlations result in reduced trust in the climate simulation. We propose an efficient supervised learning framework for DL-based parameterizations that leads to physically consistent models with improved interpretability and negligible computational overhead compared to standard supervised training. First, key features determining the target physical processes are uncovered. Subsequently, the neural network is fine-tuned using only those relevant features. We show empirically that our method robustly identifies a small subset of the inputs as actual physical drivers, therefore, removing spurious non-physical relationships. This results in by design physically consistent and interpretable neural networks while maintaining the predictive performance of standard black-box DL-based parameterizations. Our framework represents a crucial step in addressing a major challenge in data-driven climate model parameterizations by respecting the underlying physical processes, and may also benefit physically consistent deep learning in other research fields.

1 Introduction

Impacts of climate change, such as wildfires, droughts and loss of biodiversity, threaten both human well-being and the health of the planet [24]. Climate models are crucial in understanding these changes and for providing climate projections that deliver important information for mitigation and adaptation strategies [24, 25]. Climate models project climate change over several decades to hundreds of years for a variety of plausible future scenarios [38]. However, due to their complexity their horizontal grid resolution in the atmosphere

remains coarse (~40 to 100 kilometers [23]). This resolution is too coarse to explicitly simulate convective and other important small-scale processes. For instance, cloud formation takes place at scales ranging from 10 to 100 meters [35], yet these processes play a pivotal role in the climate system. Clouds transport heat and moisture and have a large impact on radiation, either by reflecting or absorbing it [7]. Thus, such unresolved subgrid-scale processes need to be parameterized in climate models [17], which forms a major source of long-standing systematic errors [13] and uncertainties in climate projections [38]. High-resolution km-scale climate models can alleviate a number of these biases [37], but due to their very high computational costs can currently not provide climate projections for multiple decades or longer [17].

A promising approach that allows long-term climate projections with models that are still fast enough to provide large ensembles, important for simulating internal variability and extremes, is the development of hybrid models. These models improve subgrid-scale parameterizations with machine learning, in particular, deep learning (DL) [17, 14]. Hybrid models, i.e., climate models coupled with DL parameterizations trained on short, high-resolution climate simulations show significantly reduced systematic errors compared to the host climate model using the traditional parameterization [33, 17, 19, 22] at substantially higher computational efficiency than high-resolution simulations [16, 21]. However, the black-box nature of DL models and their tendency to learn spurious non-physical correlations poses challenges in understanding their prediction-making processes [18, 41] and in providing out-of-distribution climate projections, leading to reduced confidence in neural network predictions. Model interpretability is especially important in Earth system sciences, where models should be consistent with our physical knowledge [39, 26]. Additionally, there is a strong interest in using these models not only for prediction but also to enhance our understanding of the physical systems being studied [10].

In this work, we introduce the Physically Consistent Masking (PC-Masking) framework, developed specifically to build predictive models that are by design physically consistent and interpretable. During the initial phase of an automated training procedure, neural networks in our PCMasking framework implicitly uncover key physical input features while learning the climate model parameterization.

* Corresponding Author. Email: birgit.kuehbacher@dlr.de

Subsequently, training focuses on fine-tuning the model weights using only physically consistent input features. The PCMasking framework is distinguished by two primary attributes. (1) The block of hidden layers depicted in Fig. 1 can be substituted with any other network architecture that matches the input/output dimensions. This adaptability positions the PCMasking framework as a versatile extension for facilitating physical driver selection not only in climate model parameterizations but also in other applications. (2) Unlike other approaches to DL-based climate model parameterization (e.g., [6, 4, 20]), the PCMasking framework is purely data-driven, requiring no prior information about physical mechanisms. This is important as subgrid-scale processes are complex and not fully understood. Iglesias-Suarez et al. [22] developed a causally-informed DL approach to achieve physical consistency without incorporating physical constraints, yet the caveat of this approach is a computationally expensive causal discovery pre-step which requires extensive domain knowledge. In contrast, PCMasking is a coherent and mostly automated framework, unique in its efficiency and usability without compromising performance in terms of prediction compared to existing techniques. Empirical evaluation with SHapley Additive exPlanations (SHAP) [30] reveals that the neural networks within the PCMasking framework successfully learn physically consistent links between the input features and the output variables.

Sec. 2 provides a brief summary of related work in the field of DL-based subgrid parameterizations. In Sec. 3, we then introduce the PCMasking framework and evaluate its offline performance using data from the Superparameterized Community Atmosphere Model v3.0 (SPCAM) [12] in Sec. 4. We conclude by discussing current limitations and interesting directions for future work.

2 Related Work

Neural networks offer a promising approach for replacing subgrid-scale physical processes in coarse-resolution climate models as they are able to learn arbitrary nonlinear functions. Methods can be broadly distinguished by examining the type of neural network, the parameterization that is to be replaced, and the kind of the data used for training. There are several examples, where fully connected feed-forward neural networks (NNs) are utilized to learn subgrid-scale processes from short high-resolution simulations and replace traditional parameterizations. Gentine et al. [16] and Rasp et al. [33] use a feed-forward NN to replace the subgrid-scale convection parameterization and radiation scheme in the Superparameterized Community Atmosphere Model v3.0 (SPCAM) [12] in an aquaplanet setup. Mooers et al. [31] investigate the offline performance of feed-forward NNs for learning clouds from high-resolution data with realistic geography. Grundner et al. [19], Henn et al. [21] present further work on cloud parameterizations by training feed-forward neural networks on coarse-grained high resolution data. Chen et al. [11] use upscaled satellite data to develop an NN-based cloud fraction parameterization. Wang et al. [40] work on a convection parameterization that uses data from multiple atmospheric model columns to improve the offline prediction of their trained neural network. Shamekh et al. [36] use a combination of an autoencoder and a standard feed-forward NN to enhance precipitation predictions from coarse-grained data, demonstrating that the prediction greatly improves when implicitly learning convective organization. While previous methods primarily employ feed-forward neural networks, making them deterministic in nature, there are also examples of stochastic parameterization approaches using neural networks. These include generative models like generative adversarial networks [32, 15] and variational autoencoders [32, 2, 3].

Although these DL-based approaches for climate model parameterizations demonstrate promising performance to varying degrees, they all suffer from a lack of interpretability and physical consistency. While some works use interpretability techniques retrospectively to understand network behavior [19, 2, 40], the primary focus remains on performance. Meanwhile, physical consistency is passively tested for, but not built into the DL models. Brenowitz et al. [8] highlight this lack of a priori interpretability as one of the limitations of machine learning based parameterizations. However, there are several examples of studies focusing on physical consistency. Beucler et al. [4] developed a physically consistent convection parameterization using a feed-forward neural network. They investigate three options: a) adapting the loss function to enforce conservation laws, b) adapting the architecture to ensure mass, energy, and radiation conservation, and c) rescaling the training and validation data to enhance generalization performance. Both Bolton and Zanna [6] and Guan et al. [20] focus on training convolutional neural networks (CNNs) with physical constraints. Bolton and Zanna [6] concentrate on reducing the momentum bias in CNNs for data-driven eddy parameterization in an ocean model. Meanwhile, Guan et al. [20] explore different strategies such as data augmentation, an architecture that preserves equivariance, and a loss function designed to maintain global enstrophy-transfer conservation. Their goal is to train a CNN for learning stable subgrid-scale closures in large-eddy simulations. Iglesias-Suarez et al. [22] aim for physical consistency and better interpretability, opting for a causal discovery method rather than incorporating physical knowledge into the NN model. They first employ constraint based causal discovery proposed by Runge et al. [34] to identify the direct causes of each variable and then train one NN predictor for each output exclusively using the identified inputs.

While these approaches represent progress in creating DL-based climate model parameterizations that are both physically consistent and interpretable, they rely heavily on either correctly integrating physical knowledge or potentially costly causal discovery in a pre-step. In this paper, we extend previous work with a neural network parameterization framework that is both physically consistent and interpretable by design. We are able to accomplish this without the need to incorporate physical knowledge into the training process or network architecture, and without the necessity for a causal discovery pre-step as in [22].

3 PCMasking Framework

The PCMasking framework is designed for training physically consistent network models for climate model parameterizations in a supervised setting. First, during the *pre-masking phase*, the input vector passes through a conventional dense input layer, then moves through an arbitrary network architecture, and ultimately reaches the output layer. This process is depicted by the blue path in Fig. 1. After a certain number of epochs, processing of the input vector is altered, as shown by the red path in Fig. 1. In this subsequent *masking phase*, certain input features are masked out by element-wise multiplication with a binary vector, with the goal of only using physically relevant inputs for the prediction. We now describe the pre-masking and masking phases in detail.

3.1 Initial Training and Finding Physical Relationships

Training in the pre-masking phase serves two purposes. Firstly, we aim to learn the value of the output variable from the input features in

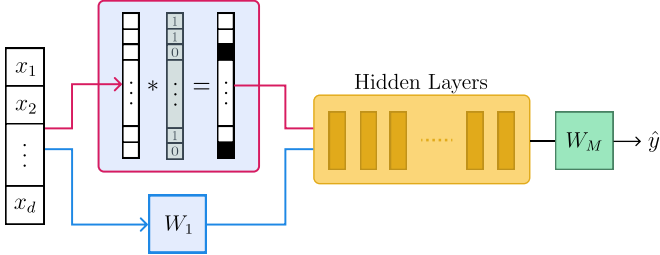


Figure 1: Schematic of a neural network model in the PCMasking framework. The blue line indicates the path of the input vector in the pre-masking phase, where it passes through a conventional dense input layer with weight matrix W_1 . In the masking phase, as illustrated by the red line, the input vector is element-wise multiplied with a masking vector. In both cases, the information then flows through an arbitrary network architecture before reaching the linear output layer with weight matrix W_M .

a supervised manner. The second goal is to implicitly learn to characterize physical relationships between the input features and the output variable. The flow of information in this stage is depicted by the blue path in Fig. 1 and we describe the network as operating in pre-mask mode.

The loss in pre-mask mode is comprised of a prediction loss in the form of the mean squared error loss and a weighted L1-regularization to encourage sparsity in the input layer weight matrix. While regularization is a common technique to prevent overfitting and increase robustness, we use sparsity regularization in particular as we expect only a limited number of inputs to be actual physical drivers of the output. The regularization term is computed as the entry-wise L1-norm, denoted by $\|vec(\cdot)\|_1$, applied to the input layer kernel W_1 . This kernel is a $(d \times d)$ -dimensional matrix, where d is the number of input features. In order to make the regularization term independent of the dimensions of W_1 , and therefore of the number of input features x_i , the L1-norm is scaled by the width and height of the kernel matrix. Thus, for input features $\mathbf{x} = (x_1, x_2, \dots, x_d)$ and target y , the optimization objective of the neural network f in pre-mask mode with parameters θ is given by

$$\operatorname{argmin}_{\theta} \frac{1}{N} \sum_{i=1}^N (y_i - f(\mathbf{x}_i; \theta))^2 + \lambda \cdot \frac{\|vec(W_1)\|_1}{d^2} \quad (1)$$

where N denotes the number of samples and λ is a regularization parameter.

After the pre-masking phase of training has finished, we automatically extract the masking vector needed for the next training phase of the PCMasking framework. We base the derivation of the masking vector on previous work by Zheng et al. [42] and Kyono et al. [28]. Zheng et al. [42] introduce a score-based approach for learning nonparametric directed acyclic graphs (DAGs) from data. Kyono et al. [28] utilize this for causal structure regularization when training a neural network model in a prediction task. It is assumed that the data generating process follows a nonparametric structural equation model of the form

$$X_i = f_i(Pa(X_i); U_i), \quad i \in \{1, 2, \dots, d\} \quad (2)$$

with random variables X_1, X_2, \dots, X_d . $Pa(X_i)$ denotes the parents, i.e., the direct causes, of X_i , and U_i noise random variable. The matrix $W(f)$ with entries

$$[W(f)]_{k,j} := \|\partial_{X_k} f_j\|_2, \quad (3)$$

then encodes the entire DAG [42], describing the conditional independence structure of the random variables X_i in Eq. 2. Here, $\|\cdot\|_2$ denotes the L2 norm. Kyono et al. [28] build the matrix $W(f)$ from the input layer weight matrices of their neural network model and use it for regularization during training. It is important to note that this method relies on the assumption that there exists a DAG between the input features X_i and the target variable Y .

While Kyono et al. [28] focus on uncovering causal connections among the entire set of variables $\{X_1, X_2, \dots, X_d, Y\}$, our methodology in the PCMasking framework is much more straightforward. We concentrate solely on the relationships between the input features X_i and the output variable Y . Consequently, we only require a d -dimensional vector which identifies related variables among the input features. Analogously to Kyono et al. [28], we extract this vector from the columns in the input layer weight matrix $W_1 = (\mathbf{w}_1 \mathbf{w}_2 \dots \mathbf{w}_d)$ as

$$\mathbf{m} := [\|\mathbf{w}_1\|_2, \|\mathbf{w}_2\|_2, \dots, \|\mathbf{w}_d\|_2]^T. \quad (4)$$

In the subsequent training phase of the PCMasking framework, this vector is used to mask any unrelated input features from influencing the output of the network.

3.2 Physically Consistent Masking and Fine-tuning

In order to reduce the number of false discoveries [42], the masking vector values are thresholded to be used in the masking phase of training, which we refer to as running the model in mask mode. The key challenge here is identifying a suitable threshold level. To address this, we suggest two approaches: Firstly, if accessible, (near) ground truth or expert knowledge can guide the choice of threshold. In the absence of such information, we propose fine-tuning the network in mask mode across various threshold values, evaluating its predictive accuracy and selecting the best performing threshold in terms of training loss. We hypothesize that, at this threshold, no essential direct physical drivers are omitted. One might expect that the lowest threshold values, which allow most inputs to pass through, result in the best predictive performance as they allow more information into the network, including possibly spurious, non-physical information. As long as there are no distributional shifts, even incidental correlation can be utilized by the network to achieve high predictive performance. However, we consistently find in our experiments that networks exhibiting the highest performance utilize larger thresholds, even though the differences in training loss are small (not shown). This indicates that using only the physical drivers of a process as inputs for the network is sufficient for predicting the process output. Once the threshold value is selected, values in the masking vector below the threshold are assigned a value of one, while all remaining values are set to zero.

After thresholding the masking vector, we continue training with fine-tuning the model weights in mask mode. The flow of information is illustrated by the red lines in Fig. 1. In mask mode, instead of passing the inputs through a traditional input layer, we perform element-wise multiplication of the input vector with the thresholded binary masking vector. Consequently, the sparsity regularization is now omitted from the optimization objective, leaving it solely defined by the mean squared error of the residuals:

$$\operatorname{argmin}_{\theta} \frac{1}{N} \sum_{i=1}^N (y_i - f(\mathbf{x}_i \odot \mathbf{m}; \theta))^2 \quad (5)$$

for a model f with parameters θ and batch size N , where \odot denotes element-wise multiplication.

There are three key aspects defining the PCMasking framework: 1) the flexibility to replace the hidden layer block shown in Fig. 1 with a different network architecture; 2) its user-friendly and efficient operation; 3) its independence from information about physical mechanisms. The capability to interchange network architectures makes the PCMasking framework a versatile tool for enhancing existing models with the capability of physical driver selection. The automation of both masking vector extraction and thresholding along with clear guidelines on threshold selection, ensure the PCMasking framework’s efficiency and ease of use. As for the framework’s independence from physical process information, we demonstrate in the following section that network models within the PCMasking framework are nevertheless capable of learning physically consistent connections between inputs and outputs.

4 Experiments

We empirically evaluate the PCMasking framework’s offline performance, i.e., how well the neural networks fit the simulation data, using high-resolution data from the Superparameterized Community Atmosphere Model v3.0 (SPCAM) [12]. This dataset and climate model were also utilized in the work by Iglesias-Suarez et al. [22], providing a baseline comparison for our PCMasking framework. Iglesias-Suarez et al. [22] employ constraint based causal discovery [34] as a pre-step to determine the direct causes of each variable. Subsequently, they construct a single-output neural network for each variable, including only the identified causes as network inputs. Although this approach results in more interpretable DL-based parameterizations, the causal discovery method used is computationally expensive, relies on causal assumptions, and introduces its own hyper-parameters that require expert domain knowledge to tune. In this section, we demonstrate that the PCMasking framework enables us to achieve comparable offline prediction accuracy and physical consistency as Iglesias-Suarez et al. [22], while being more efficient and largely automated. In fact, the overall resource consumption of the PCMasking framework is only about half of what is required for just the causal discovery pre-step, provided both methods are already tuned (see Supporting Information Text S1 for details). The training times of the PCMasking framework networks and the causally-informed NNs are approximately the same, making the PCMasking framework three times more efficient overall compared to the method proposed by Iglesias-Suarez et al. [22]. In the following, we will briefly outline the SPCAM setup and the neural network configuration followed by a presentation of our experimental results.

4.1 SPCAM and Neural Network Configuration

SPCAM is a high-resolution global circulation model composed of the Community Atmosphere Model (CAM) with an embedded superparameterization component – a 2D storm-resolving model (SRM) within each grid column. This embedded SRM, the SP component, features eight north-south oriented 4 km-wide columns and explicitly resolves the majority of deep convective processes, while relying on parameterizations for turbulence and microphysics. Following Iglesias-Suarez et al. [22], we use SPCAM data from an aquaplanet setup, meaning there is only ocean and no topography. The sea surface temperatures are fixed, featuring a realistic equator-to-pole gradient [1], and a diurnal cycle without seasonal changes. The model spans from the surface to the upper stratosphere at 3.5 hPa, encompassing 30 vertical levels and a horizontal grid resolution of 2.8° in both latitude and longitude. CAM operates with a time step of 30

minutes, while the embedded SRM uses a time step of 20 seconds. For further information on SPCAM and the climate model setup, we refer the reader to Iglesias-Suarez et al. [22] and its Supplementary Information.

SPCAM Data The neural network is tasked to learn the subgrid-scale processes at each time step as represented by the SP component, based on the atmospheric state provided by the general circulation model (CAM). The training dataset covers the SP subgrid resolution of convection and radiation, though with some omissions (e.g., condensates). The neural network inputs are comprised of column-wise values of temperature $T(p)$, specific humidity $q(p)$, and meridional wind $V(p)$ at every vertical level p (3D variables, $p \in \{0, \dots, 29\}$), as well as surface pressure P_{srf} , incoming solar radiation Q_{sol} at the top of the atmosphere, and sensible-heat flux Q_{sen} and latent-heat flux Q_{lat} at the surface (2D variables). The outputs include heating tendencies $\Delta T_{phy}(p)$ and moistening tendencies $\Delta q_{phy}(p)$ at each vertical level p , as well as net shortwave and longwave radiative heat fluxes at the model top and at the surface, Q_{sw}^{top} , Q_{lw}^{top} , Q_{sw}^{srf} , and Q_{lw}^{srf} , respectively, and surface precipitation P . The input and output variables are arranged into vectors, with the input vector $\mathbf{x} = [q, T, V, P_{srf}, Q_{sol}, Q_{sen}, Q_{lat}]^T$ having a length of 94, and the output vector $\mathbf{y} = [\Delta q_{phy}, \Delta T_{phy}, Q_{sw}^{top}, Q_{sw}^{srf}, Q_{lw}^{top}, Q_{lw}^{srf}, P]^T$ consisting of 65 elements. It is important to note that in masking mode only a fraction of the inputs is actually processed by the network. The input values are standardized and the outputs are normalized to ensure a similar order of magnitude (see Supporting Information Tab. S1). We use simulation data from SPCAM spanning three months each for training, validation, and testing, yielding about 45 million data samples for each dataset. The training data is shuffled in both time and space (across grid columns).

Neural Network Configuration For most of the neural network and hyper-parameter configurations, we follow Iglesias-Suarez et al. [22] to ensure comparability of our results. To identify the physical drivers for each output variable, we construct one single-output neural network per variable, resulting in 65 neural networks in total. Each model incorporates the same block of hidden layers, comprising nine fully-connected layers with 256 units each. These layers employ Leaky Rectified Linear Unit (ReLU) activation with a negative slope of 0.3. The initial learning rate is set to 0.001, which is divided by five every three epochs. The training batch size is 1024 and the models are optimized using the ADAM optimizer [27] with default parameters. For validation and testing, the batch size is increased to 8192, covering all grid cells of the aquaplanet. We carry out hyper-parameter tuning for the sparsity loss weighting coefficient, λ , in pre-mask mode (see Eq. 1). Exploring a log-spaced search grid $\{1.0, 0.1, \dots, 1 \times 10^{-5}\}$, we find that $\lambda = 0.001$ yields the best outcomes in both prediction accuracy and physical consistency of the identified relevant input features (see Supporting Information Fig. S1). While we use the same λ for all models, the masking vector and the threshold selection are customized for each individual output. To determine the threshold for a masking vector \mathbf{m} , we fine-tune the neural network in mask mode with 20 distinct threshold values. The thresholds are evenly distributed within the interval $[1 \times 10^{-4}, p_{70})$, where p_{70} represents the 70th percentile of the values in \mathbf{m} . We round these values to four decimal places. Once the fine-tuning for each threshold value is complete, we proceed to analyzing the training loss for each threshold. We then select the model with the best performance for each variable. Training is carried out on a single NVIDIA A100 Tensor Core GPU, equipped with 40 GB memory.

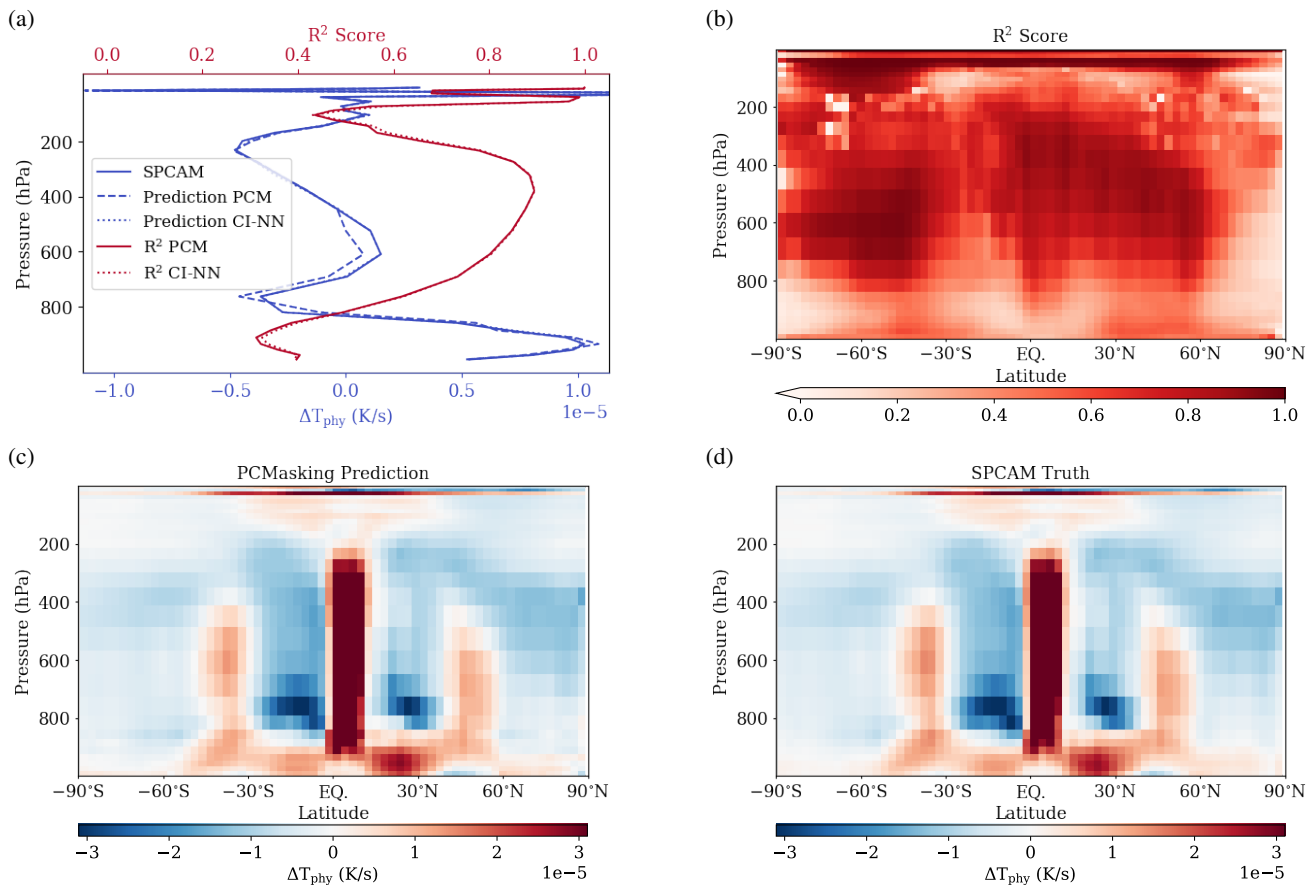


Figure 2: PCMasking framework offline evaluation for temperature tendency ΔT_{phy} with $\lambda = 0.001$ and thresholds selected based on best training loss performance among 20 thresholds from the interval $[1 \times 10^{-4}, p_{70})$. One neural network model is trained for each of the 30 vertical levels. All values are averaged for 1440 test data samples. See Supporting Information Fig. S2 for results for output variable moistening tendency Δq_{phy} . (a) Horizontally averaged vertical profiles for SPCAM truth, prediction and R^2 for causally-informed neural network (CI-NN) and our PCMasking framework (PCM). (b) Vertical cross-section R^2 for PCMasking framework. (c) Vertical cross-section for PCMasking framework prediction. (d) Vertical cross-section SPCAM truth.

For comparability with Iglesias-Suarez et al. [22], we also train for 18 epochs in total, which we split evenly into 9 epochs training in pre-mask mode and 9 epochs fine-tuning in mask mode. The training time in pre-mask mode is roughly 45 minutes for each network (around 0.56 million parameters), while a single fine-tuning run takes approximately 40 minutes per network (around 0.55 million parameters).

4.2 Experimental Results

To determine the PCMasking framework’s suitability for efficient physically consistent data-driven climate model parameterization, we evaluate its offline performance on the SPCAM test dataset in terms of both predictive performance and physical consistency.

Offline Predictive Performance Figures 2c and 2d show pressure-latitude cross-sections of the average predicted and actual SPCAM heating tendencies, respectively, across 1440 samples (about one month). The neural networks of the PCMasking framework effectively capture the heating tendency in terms of horizontal and vertical structure, accurately representing key features such as the Intertropical Convergence Zone (ITCZ), evident as the dark red column at the equator, and the heating patterns of mid-latitude storm tracks, depicted in light red, at the correct geographical locations. Moreover,

there are no strong heating patterns at the poles due to cold and dry air which limits convective activity. The horizontal lines at the top of the atmosphere are mostly related to incoming solar radiation.

In order to examine the predictive performance more closely, we turn to the coefficient of determination, R^2 , calculated as one minus the ratio of the residual sum of squares and the total sum of squares. The statistical measure serves as a goodness-of-fit quantifier, indicating the extent to which the variance in the dependent variable (the model output y) can be explained by the independent variable (the model input x). An R^2 score of 1 means that the predicted values exactly match the observed ones, meaning that the model accounts for all variability in the data. Conversely, an R^2 score of 0 implies that the model does no better than simply predicting the mean.

Fig. 2b displays a pressure-latitude cross-section of the R^2 score for temperature tendency. It reveals patches with particularly strong predictive skills near 600 hPa at the equator and in the mid-latitudes, aligning with the locations of the ITCZ and mid-latitude storm tracks. However, the predictive performance noticeably declines in the lower troposphere (around 700-1000 hPa), particularly within the planetary boundary layer. This reduced performance is likely associated with turbulent and stochastic processes in the planetary boundary layer, leading to increased noise and stochasticity in the data, as previously documented in studies such as [16, 22, 3]. By design, this

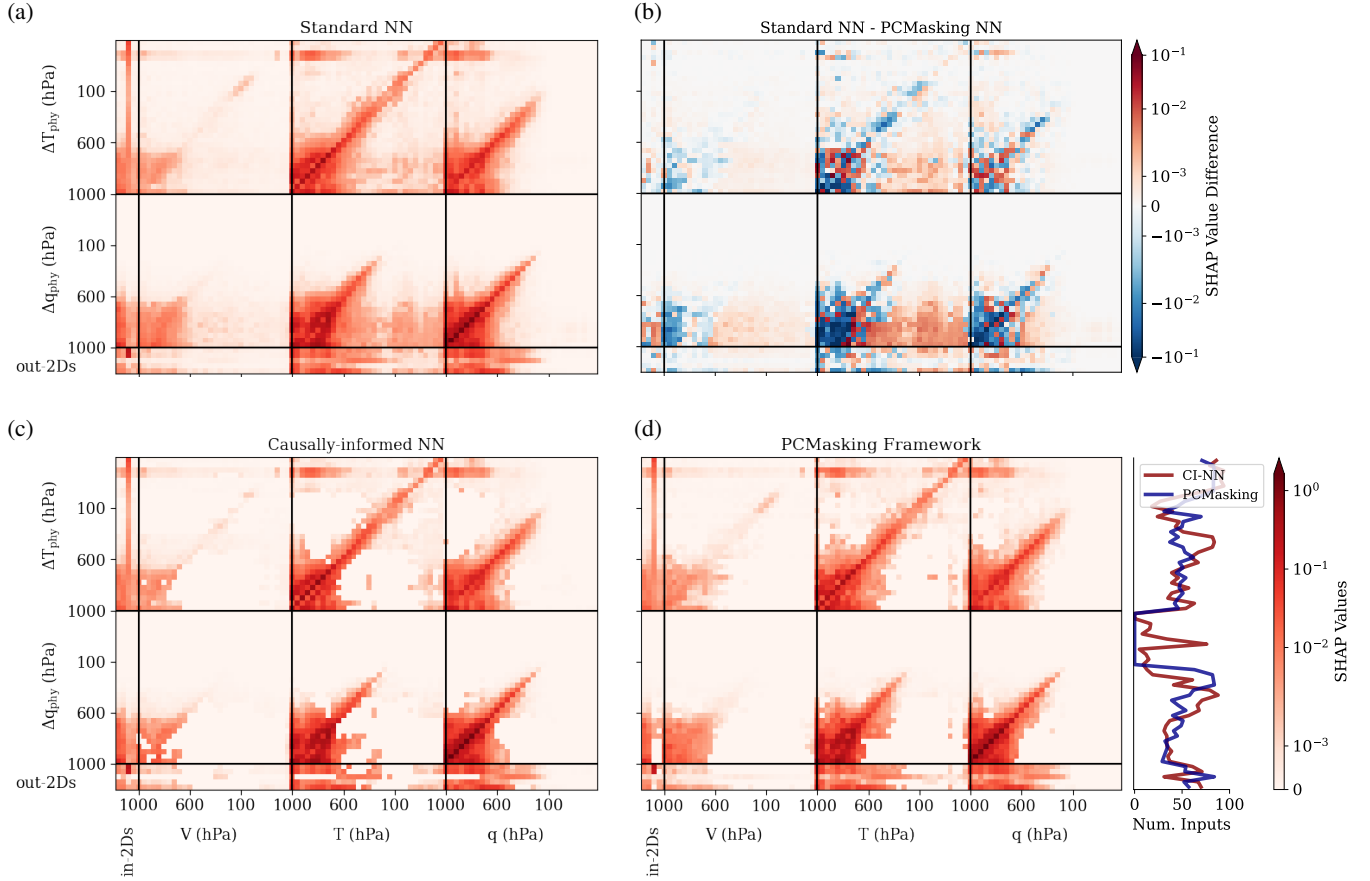


Figure 3: Absolute SHAP value comparison for vanilla feed-forward neural networks (NNs), causally-informed NNs [22] and PCMasking framework NNs. The PCMasking networks were trained with $\lambda = 0.001$ and thresholds were selected based on best training loss performance among 20 thresholds from the interval $[1 \times 10^{-4}, p_{70})$. 1000 data samples were used for SHAP computation. (a) Absolute SHAP values for vanilla feed-forward NNs. (b) Absolute SHAP value difference between vanilla feed-forward NNs and the PCMasking NNs. (c) Absolute SHAP values for causally-informed NNs. (d) Absolute SHAP values for NNs trained in the PCMasking framework.

stochasticity cannot be captured by a deterministic neural network. The fact that the deterministic neural network’s predictions are more smoothed out compared to SPCAM is evident when looking at snap shots instead of averaged data (see Supporting Information Fig. S3). The performance drop-off in the lower troposphere is also visible in Fig. 2a which shows the horizontal averages of the prediction of the causally-informed neural network (CI-NN) [22], the prediction of the neural network trained in the PCMasking framework (PCM), the SPCAM truth, and the R^2 scores for both networks. The performance of CI-NN is equivalent to that of a standard fully-connected feed-forward neural network (not shown, see [22]). Our predictive performance closely aligns with that of CI-NN, including similar limitations in the lower atmosphere where reliable prediction is particularly challenging due to stochasticity, as previously discussed. Moreover, the PCMasking framework consumes about two-thirds fewer resources than CI-NN, making it significantly more efficient while maintaining nearly the same level of performance.

Physical Consistency and Interpretability For evaluation in terms of interpretability and physical consistency, we turn to SHapley Additive exPlanations (SHAP) [30], a framework for explaining the output of machine learning models. Based on the concept of Shapley values from game theory, SHAP values measure the contribution of each feature to the prediction for each data sample, thus providing in-

sight into how each feature influences the model’s decision-making process. Figures 3a, 3c, and 3d show the absolute mean SHAP values for a vanilla fully-connected feed-forward neural network, CI-NN [22], and our PCMasking framework, respectively. The plots depict which input variables (on the x-axis) the networks are using for the prediction of the output variables (on the y-axis). The values are computed from 1000 data samples.

Based on physical knowledge about the climate system, we know that in the lower troposphere, interactions are generally both local and non-local due to mixing in the planetary boundary layer and buoyancy plumes from the surface. Conversely, in the upper troposphere (around 100-300 hPa) and stratosphere (above 100 hPa), processes are predominantly local. Fig. 3a clearly illustrates that the vanilla feed-forward NNs, which utilize all inputs for predictions, exhibit numerous connections between inputs throughout the atmosphere, especially temperature, and heating and moistening tendencies in the lower troposphere. Such non-local interactions somewhat conflict with our physical understanding, i.e., convection is mainly driven by processes within the troposphere, such as adiabatic cooling and heating, cloud formation, and latent heat release during phase changes of water. This suggests that these are spurious connections likely learned due to vertical correlation in the atmosphere due to convective processes. In contrast, Figures 3c and 3d both demonstrate that CI-NN and our PCMasking framework successfully re-

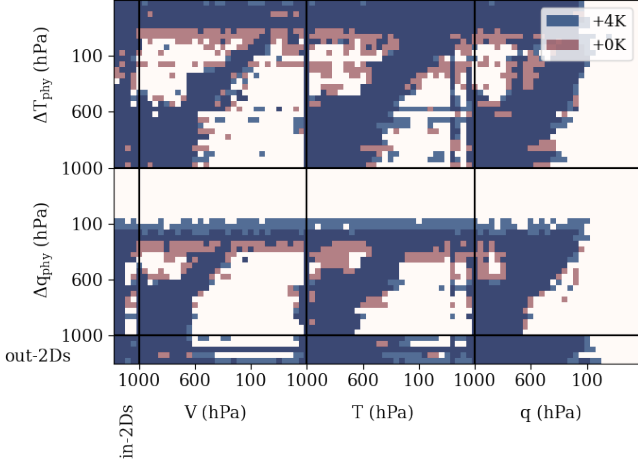


Figure 4: Comparison of physical driver selection for 0 K reference climate and +4 K climate in the PCMasking framework. The neural networks were trained with $\lambda = 0.001$ and thresholds were selected based on best training loss performance among 20 thresholds from the interval $[1 \times 10^{-4}, p_{70})$. See Supporting Information S4 for comparison of 0 K and +4 K climates.

move these spurious links. This is further highlighted in the SHAP difference between the vanilla NN and the PCMasking framework in Fig. 3b. All red areas indicate positive values, meaning that these input-output links were more pronounced in the standard NN. Conversely, negative, blue values indicate these connections are more prominent in the PCMasking framework. The elimination of spurious links in the PCMasking framework is particularly evident for input variable temperature, as indicated by the red areas in Fig. 3b. Furthermore, this removal of spurious connections results in greater focus on the connections between subgrid-scale processes and the actual physical drivers in the PCMasking framework. This is evidenced by the blue areas for both non-local and local interactions in the lower troposphere as well as for local interactions along the diagonal.

Moreover, Fig. 3d depicts the number of inputs identified by CI-NN and the PCMasking framework at each vertical level for moistening and temperature tendencies. Although the overall patterns of peaks and valleys are similar, there is a notable difference: the PCMasking framework successfully avoids to identify any input variables in the stratosphere for moistening tendency. This is expected due to the dry air and the absence of most convective processes in the stratosphere. Overall, the SHAP value comparison between the three types of networks conclusively demonstrates two key points: 1) both CI-NN and the PCMasking framework effectively remove non-physical, spurious links, and 2) in doing so, networks within the PCMasking framework focus on actual physical connections in their predictions. Consequently, the resulting neural network models are both physically consistent and interpretable.

Evaluation on Different Climates In order to demonstrate the ability of our PCMasking framework to consistently identify physical drivers across different climates, we trained on different SPCAM simulations with sea surface temperatures of +4 K and -4 K compared to the reference climate (+0 K). Fig. 4 presents the number of inputs found in both the reference climate (+0K) and the warmed climate (+4K). While the local and non-local drivers in the lower troposphere remain the same across both climates, there is a noticeable upward shift of moistening tendencies, occurring at approximately 100 hPa. This is consistent with deep convective processes occurring at higher altitudes in warmer climates, further providing strong

evidence that our PCMasking framework is indeed identifying real-world physical drivers. However, the slight change in physical drivers also indicates that achieving good generalization across different climates using this methodology may be limited to some extent. This warrants exploration of generalization performance in future work.

5 Conclusion

Prior work as shown that DL-based climate model parameterizations are able to improve climate model simulations over traditional non-data driven parameterization schemes (e.g. [33, 19]). However, deep neural networks are black-box models that rely on statistical correlations in the training data to generate a prediction. In climate science, this leads to reduced model trust and reluctance to incorporate DL-based parameterizations into physical models [26]. In this work, we introduce the PCMasking framework, an efficient training scheme that results in physically consistent and interpretable neural network models, specifically designed for climate model parameterization. We have demonstrated empirically that the PCMasking framework reliably identifies real-world physical drivers of convective processes across different climate conditions without relying on physical constraints. Furthermore, networks trained with the PCMasking framework are competitive with previous work [22] in terms of offline predictive performance, with only a third of the computational cost. The PCMasking framework features an automated training process, making it efficient and easy to use. Moreover, the interchangeability of its internal architecture, makes the PCMasking framework a versatile tool for enhancing predictive models with physical driver selection. Possible other applications may well be forecasting air pollutants or predicting sea ice concentrations in a climate model. More broadly, the PCMasking framework may be useful outside of climate science, for example, in identifying and quantifying gene regulatory effects in single-cell RNA measurements.

While this study is a great step towards physically consistent deep neural network models for climate model parameterizations, there are still several challenges that remain to be addressed. These include generalization to different climates and online stability, i.e., the stability of hybrid model climate simulations [29]. Tackling the problem of generalization, Beucler et al. [5] propose a strategy of transforming the inputs and outputs to maintain similar distributions under different climate conditions. This could readily be integrated into our PCMasking framework. Moreover, the transition from offline to online performance is a major challenge in data-driven DL-based parameterizations, as success in offline settings does not always translate to coupled model runs [9, 29]. Brenowitz et al. [8] suggest that the numerical instabilities commonly observed in coupled model runs could be related to non-causal correlations or sub-optimal selections of network architecture and hyper-parameters. However, non-causal correlations have not been found to be closely related to hybrid model instabilities [22]. This is a key challenge in hybrid modeling and remains an active area of research.

Overall, we demonstrate that the PCMasking framework represents an innovative step in addressing a major challenge of data-driven models by respecting the underlying physical processes of the data. Our framework advances the process-based representation of complex phenomena. Given its flexibility and applicability to other predictive tasks, it can benefit not just climate science but other scientific disciplines as well.

Acknowledgements

Funding for this study was provided by the European Research Council (ERC) Synergy Grant “Understanding and modeling the Earth System with Machine Learning (USMILE)” under the Horizon 2020 research and innovation programme (Grant Agreement 855187). This work used resources of both the Deutsches Klimarechenzentrum (DKRZ) granted by its Scientific Steering Committee (WLA) under project ID 1179 (USMILE), and the supercomputer JUWELS at the Jülich Supercomputing Centre (JSC) under the “Machine learning-based parameterizations and analysis for the ICON model” project.

References

- [1] J. A. Andersen and Z. Kuang. Moist Static Energy Budget of MJO-like Disturbances in the Atmosphere of a Zonally Symmetric Aquaplanet. *Journal of Climate*, 25(8):2782–2804, Apr. 2012. doi: 10/bqx6cx.
- [2] G. Behrens, T. Beucler, P. Gentine, F. Iglesias-Suarez, M. Pritchard, and V. Eyring. Non-Linear Dimensionality Reduction With a Variational Encoder Decoder to Understand Convective Processes in Climate Models. *Journal of Advances in Modeling Earth Systems*, 14(8), 2022. doi: 10/gtqrjg.
- [3] G. Behrens, T. Beucler, F. Iglesias-Suarez, S. Yu, P. Gentine, M. Pritchard, M. Schwabe, and V. Eyring. Improving Atmospheric Processes in Earth System Models with Deep Learning Ensembles and Stochastic Parameterizations, Feb. 2024.
- [4] T. Beucler, M. Pritchard, P. Gentine, and S. Rasp. Towards Physically-Consistent, Data-Driven Models of Convection. In *IGARSS 2020 - 2020 IEEE International Geoscience and Remote Sensing Symposium*, pages 3987–3990, Sept. 2020. doi: 10/gtn9pz.
- [5] T. Beucler, P. Gentine, J. Yuval, A. Gupta, L. Peng, J. Lin, S. Yu, S. Rasp, F. Ahmed, P. A. O’Gorman, J. D. Neelin, N. J. Lutsko, and M. Pritchard. Climate-invariant machine learning. *Science Advances*, 10(6), Feb. 2024. doi: 10/gtn9v8.
- [6] T. Bolton and L. Zanna. Applications of Deep Learning to Ocean Data Inference and Subgrid Parameterization. *Journal of Advances in Modeling Earth Systems*, 11(1):376–399, 2019. doi: 10/gfsvqg.
- [7] O. Boucher, D. Randall, P. Artaxo, C. Bretherton, G. Feingold, P. Forster, V. Kerminen, Y. Kondo, H. Liao, U. Lohmann, et al. Clouds and Aerosols. In *Climate Change 2013 – The Physical Science Basis: Working Group I Contribution to the Fifth Assessment Report of the Intergovernmental Panel on Climate Change*, page 571–658. Cambridge University Press, Cambridge, United Kingdom and New York, NY, USA, 2014. doi: 10.1017/CBO9781107415324.016.
- [8] N. D. Brenowitz, T. Beucler, M. Pritchard, and C. S. Bretherton. Interpreting and Stabilizing Machine-Learning Parameterizations of Convection. *Journal of the Atmospheric Sciences*, 77(12):4357–4375, Dec. 2020. doi: 10/grspqj.
- [9] N. D. Brenowitz, B. Henn, J. McGibbon, S. K. Clark, A. Kwa, W. A. Perkins, O. Watt-Meyer, and C. S. Bretherton. Machine Learning Climate Model Dynamics: Offline versus Online Performance, Nov. 2020.
- [10] G. Camps-Valls, M. Reichstein, X. Zhu, and D. Tuia. Advancing Deep Learning for Earth Sciences: From Hybrid Modeling to Interpretability. In *IGARSS 2020 - 2020 IEEE International Geoscience and Remote Sensing Symposium*, pages 3979–3982, Sept. 2020. doi: 10/gsczrb.
- [11] G. Chen, W.-C. Wang, S. Yang, Y. Wang, F. Zhang, and K. Wu. A Neural Network-Based Scale-Adaptive Cloud-Fraction Scheme for GCMs. *Journal of Advances in Modeling Earth Systems*, 15(6), 2023. doi: 10/gtn9pm.
- [12] W. D. Collins, P. J. Rasch, B. A. Boville, J. J. Hack, J. R. McCaa, D. L. Williamson, B. P. Briegleb, C. M. Bitz, S.-J. Lin, and M. Zhang. The Formulation and Atmospheric Simulation of the Community Atmosphere Model Version 3 (CAM3). *Journal of Climate*, 19(11):2144–2161, June 2006. doi: 10/c28trn.
- [13] V. Eyring, N. Gillett, K. A. Rao, R. Barimalala, M. B. Parrillo, N. Bellouin, C. Cassou, P. Durack, Y. Kosaka, S. McGregor, S. Min, O. Morgenstern, and Y. Sun. Human Influence on the Climate System. In V. Masson-Delmotte, P. Zhai, A. Pirani, S. Connors, C. Péan, S. Berger, N. Caud, Y. Chen, L. Goldfarb, M. Gomis, M. Huang, K. Leitzell, E. Lonnoy, J. Matthews, T. Maycock, T. Waterfield, O. Yelekçi, R. Yu, , and B. Zhou, editors, *Climate Change 2021: The Physical Science Basis. Contribution of Working Group I to the Sixth Assessment Report of the Intergovernmental Panel on Climate Change*, chapter 3, page 423–552. Cambridge University Press, Cambridge, United Kingdom and New York, NY, USA, 2021. URL <https://www.ipcc.ch/report/ar6/wgl/>.
- [14] V. Eyring, P. Gentine, G. Camps-Valls, D. M. Lawrence, and M. Reichstein. Ai-empowered next-generation multiscale climate modeling for mitigation and adaptation. *Nature Geoscience*, 2024, in review.
- [15] D. J. Gagne II, H. M. Christensen, A. C. Subramanian, and A. H. Monahan. Machine Learning for Stochastic Parameterization: Generative Adversarial Networks in the Lorenz ’96 Model. *Journal of Advances in Modeling Earth Systems*, 12(3), 2020. doi: 10/gg4z5t.
- [16] P. Gentine, M. Pritchard, S. Rasp, G. Reinaudi, and G. Yacalis. Could Machine Learning Break the Convection Parameterization Deadlock? *Geophysical Research Letters*, 45(11):5742–5751, 2018. doi: 10/gdnfbs.
- [17] P. Gentine, V. Eyring, and T. Beucler. Deep Learning for the Parameterization of Subgrid Processes in Climate Models. In *Deep Learning for the Earth Sciences*, chapter 21, pages 307–314. John Wiley & Sons, Ltd, 2021. doi: 10.1002/9781119646181.ch21.
- [18] L. H. Gilpin, D. Bau, B. Z. Yuan, A. Bajwa, M. Specter, and L. Kagal. Explaining Explanations: An Overview of Interpretability of Machine Learning. In *2018 IEEE 5th International Conference on Data Science and Advanced Analytics (DSAA)*, pages 80–89, Oct. 2018. doi: 10.1109/DSAA.2018.00018.
- [19] A. Grundner, T. Beucler, P. Gentine, F. Iglesias-Suarez, M. A. Giorgetta, and V. Eyring. Deep Learning Based Cloud Cover Parameterization for ICON. *Journal of Advances in Modeling Earth Systems*, 14(12), 2022. doi: 10/gs5rbs.
- [20] Y. Guan, A. Subel, A. Chattopadhyay, and P. Hassanzadeh. Learning physics-constrained subgrid-scale closures in the small-data regime for stable and accurate LES. *Physica D: Nonlinear Phenomena*, 443: 133568, Jan. 2023. doi: 10/gq9kr4.
- [21] B. Henn, Y. R. Jauregui, S. K. Clark, N. D. Brenowitz, J. McGibbon, O. Watt-Meyer, A. G. Pauling, and C. S. Bretherton. A Machine Learning Parameterization of Clouds in a Coarse-Resolution Climate Model for Unbiased Radiation. *Journal of Advances in Modeling Earth Systems*, 16(3), 2024. doi: 10.1029/2023MS003949.
- [22] F. Iglesias-Suarez, P. Gentine, B. Solino-Fernandez, T. Beucler, M. Pritchard, J. Runge, and V. Eyring. Causally-Informed Deep Learning to Improve Climate Models and Projections. *Journal of Geophysical Research: Atmospheres*, 129(4), 2024. doi: 10/gtmfjk.
- [23] Intergovernmental Panel on Climate Change (IPCC). Annex II: Models. In V. Masson-Delmotte, P. Zhai, A. Pirani, S. Connors, C. Péan, S. Berger, N. Caud, Y. Chen, L. Goldfarb, M. Gomis, M. Huang, K. Leitzell, E. Lonnoy, J. Matthews, T. Maycock, T. Waterfield, O. Yelekçi, R. Yu, , and B. Zhou, editors, *Climate Change 2021: The Physical Science Basis. Contribution of Working Group I to the Sixth Assessment Report of the Intergovernmental Panel on Climate Change*, Gutiérrez, J M., A.-M. Tréguier (eds.), page 2087–2138. Cambridge University Press, Cambridge, United Kingdom and New York, NY, USA, 2021. URL <https://www.ipcc.ch/report/ar6/wgl/>.
- [24] IPCC. *Climate Change 2021 – The Physical Science Basis: Working Group I Contribution to the Sixth Assessment Report of the Intergovernmental Panel on Climate Change*. Cambridge University Press, Cambridge, 2023. doi: 10.1017/9781009157896.
- [25] IPCC. *Climate Change 2023: Synthesis Report. Contribution of Working Groups I, II and III to the Sixth Assessment Report of the Intergovernmental Panel on Climate Change*, chapter Summary for Policymakers. Cambridge University Press, Cambridge, United Kingdom and New York, NY, USA, 2023. doi: 10.59327/IPCC/AR6-9789291691647.001. Core Writing Team, H. Lee and J. Romero (eds.).
- [26] K. Kashinath, M. Mustafa, A. Albert, J.-L. Wu, C. Jiang, S. Esmaeilzadeh, K. Azizzadenesheli, R. Wang, A. Chattopadhyay, A. Singh, A. Manepalli, D. Chirila, R. Yu, R. Walters, B. White, H. Xiao, H. A. Tchelepi, P. Marcus, A. Anandkumar, P. Hassanzadeh, and n. Prabhath. Physics-informed machine learning: Case studies for weather and climate modelling. *Philosophical Transactions of the Royal Society A: Mathematical, Physical and Engineering Sciences*, 379(2194), Feb. 2021. doi: 10/gjw27t.
- [27] D. P. Kingma and J. Ba. Adam: A Method for Stochastic Optimization, Jan. 2017.
- [28] T. Kyono, Y. Zhang, and M. van der Schaar. CASTLE: Regularization via Auxiliary Causal Graph Discovery. In *Advances in Neural Information Processing Systems*, volume 33, pages 1501–1512. Curran Associates, Inc., 2020.
- [29] J. Lin, S. Yu, T. Beucler, P. Gentine, D. Walling, and M. Pritchard. Systematic Sampling and Validation of Machine Learning-Parameterizations in Climate Models, Sept. 2023.
- [30] S. M. Lundberg and S.-I. Lee. A Unified Approach to Interpreting

- Model Predictions. In *Advances in Neural Information Processing Systems*, volume 30. Curran Associates, Inc., 2017.
- [31] G. Mooers, M. Pritchard, T. Beucler, J. Ott, G. Yacalis, P. Baldi, and P. Gentine. Assessing the Potential of Deep Learning for Emulating Cloud Superparameterization in Climate Models With Real-Geography Boundary Conditions. *Journal of Advances in Modeling Earth Systems*, 13(5), 2021. doi: 10/gmhqft.
- [32] P. Perezhogin, L. Zanna, and C. Fernandez-Granda. Generative Data-Driven Approaches for Stochastic Subgrid Parameterizations in an Idealized Ocean Model. *Journal of Advances in Modeling Earth Systems*, 15(10), 2023. doi: 10/gtn9tt.
- [33] S. Rasp, M. S. Pritchard, and P. Gentine. Deep learning to represent sub-grid processes in climate models. *Proceedings of the National Academy of Sciences*, 115(39):9684–9689, Sept. 2018. doi: 10/gfcpxb.
- [34] J. Runge, P. Nowack, M. Kretschmer, S. Flaxman, and D. Sejdinovic. Detecting and quantifying causal associations in large nonlinear time series datasets. *Science Advances*, 5(11), Nov. 2019. doi: 10/ggd3s5.
- [35] T. Schneider, J. Teixeira, C. S. Bretherton, F. Briant, K. G. Pressel, C. Schär, and A. P. Siebesma. Climate goals and computing the future of clouds. *Nature Climate Change*, 7(1):3–5, Jan. 2017. doi: 10/gf9pkz.
- [36] S. Shamekh, K. D. Lamb, Y. Huang, and P. Gentine. Implicit learning of convective organization explains precipitation stochasticity. *Proceedings of the National Academy of Sciences*, 120(20), May 2023. doi: 10/gr9bvt.
- [37] B. Stevens, M. Satoh, L. Auger, J. Biercamp, C. S. Bretherton, X. Chen, P. Düben, F. Judt, M. Khairoutdinov, D. Klocke, and et al. DYAMOND: The DYNamics of the Atmospheric general circulation Modeled On Non-hydrostatic Domains. *Progress in Earth and Planetary Science*, 6(1), Sept. 2019. doi: 10/gmfk2q.
- [38] C. Tebaldi, K. Debeire, V. Eyring, E. Fischer, J. Fyfe, P. Friedlingstein, R. Knutti, J. Lowe, B. O’Neill, B. Sanderson, and et al. Climate model projections from the Scenario Model Intercomparison Project (ScenarioMIP) of CMIP6. *Earth System Dynamics*, 12(1):253–293, Mar. 2021. doi: 10/gh6k9m.
- [39] B. A. Toms, E. A. Barnes, and I. Ebert-Uphoff. Physically Interpretable Neural Networks for the Geosciences: Applications to Earth System Variability. *Journal of Advances in Modeling Earth Systems*, 12(9), 2020. doi: 10/gg9n6m.
- [40] P. Wang, J. Yuval, and P. A. O’Gorman. Non-Local Parameterization of Atmospheric Subgrid Processes With Neural Networks. *Journal of Advances in Modeling Earth Systems*, 14(10), 2022. doi: 10/gqrjx9.
- [41] Y. Zhang, P. Tiño, A. Leonardis, and K. Tang. A Survey on Neural Network Interpretability. *IEEE Transactions on Emerging Topics in Computational Intelligence*, 5(5):726–742, Oct. 2021. doi: 10/gmq3gq.
- [42] X. Zheng, C. Dan, B. Aragam, P. Ravikumar, and E. Xing. Learning Sparse Nonparametric DAGs. In *Proceedings of the Twenty Third International Conference on Artificial Intelligence and Statistics*, pages 3414–3425. PMLR, June 2020.

Supporting Information

Text S1: Computing Time Comparison We compared computing resources of our PCMasking framework and the causally-informed neural networks (NNs) presented by Iglesias-Suarez et al. [22]. The run time and resource consumption for all neural network types (standard feed-forward NN, causally-informed NN [22], and our PCMasking framework) are about the same. Using all 4 GPUs on an HPC compute node (GPUs: 4x Nvidia A100 80GB/GPU2x AMD 7763 CPU; CPUs: 128 cores in total, 512 GB main memory), training all 65 networks consumes ~25 node-hours (~0.38 node-hours per output variable).

Iglesias-Suarez et al. [22] require additional resources for their causal discovery pre-step, for which they use the constraint-based PC₁ algorithm of PCMI framework [34]. PC₁ takes ~46 seconds per grid cell for the SPCAM dataset (2x AMD 7763 CPU; 128 cores in total, 256 GB main memory). The SPCAM grid has 8192 grid cells (128 longitudes × 64 latitudes). Assuming one can run PC₁ perfectly and efficiently using a compute node (128 jobs in parallel with 1 job per core), we estimate the computation for PC₁ as: 65 outputs × 64 jobs (8192 column / 128 cores) × 46 seconds ≈ 53 additional node-hours (~0.81 node-hours per output variable).

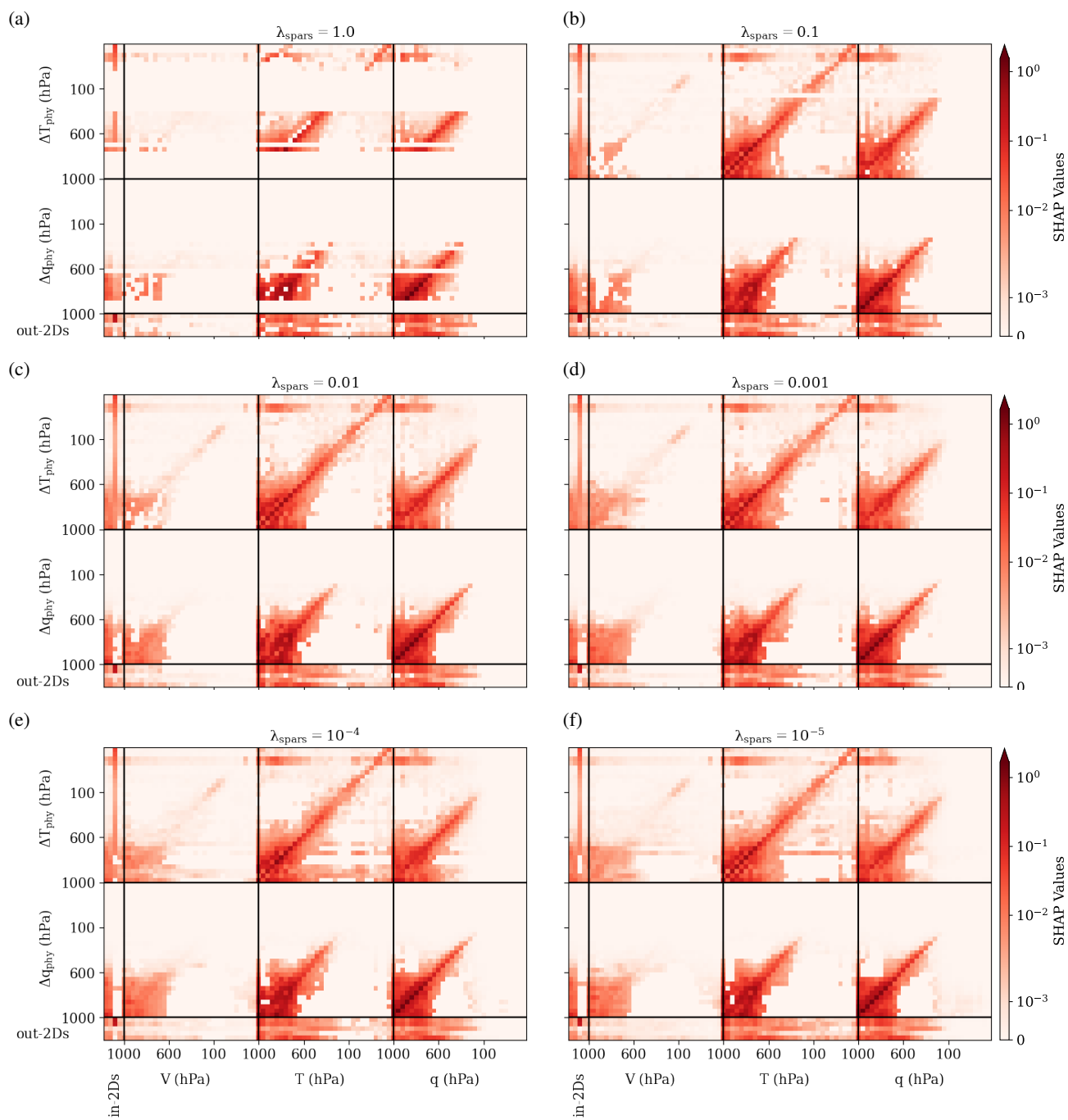
Thus, CI-NN requires 3x more computing resources compared to our PCMasking framework.

Table S1: Summary of neural networks input and output variables. The values are equivalent to [22]. The input variables are standardized and the output values are normalized.

Inputs	Units	Outputs	Units	Normalization
Temperature, $T(p)$	K	Temperature tendencies, $\Delta T_{phy}(p)$	$K s^{-1}$	C_p
Specific humidity, $q(p)$	$kg kg^{-1}$	Moistening tendencies $\Delta q_{phy}(p)$	$kg kg^{-1} s^{-1}$	L_v
Meridional wind, $V(p)$	$m s^{-1}$	Net shortwave radiative heat flux at TOA, Q_{sw}^{top}	$W m^{-2}$	10^{-3}
Surface pressure, P_{surf}	Pa	Net longwave radiative heat flux at TOA, Q_{lw}^{top}	$W m^{-2}$	10^{-3}
Incoming solar radiation, Q_{sol}	$W m^{-2}$	Net shortwave radiative heat flux at the surface, Q_{sw}^{surf}	$W m^{-2}$	10^{-3}
Sensible heat flux, Q_{sen}	$W m^{-2}$	Net longwave radiative heat flux at the surface, Q_{lw}^{surf}	$W m^{-2}$	10^{-3}
Latent heat flux, Q_{lat}	$W m^{-2}$	Precipitation, P	$kg m^{-2} d^{-1}$	1.728×10^6

Table S2: Neural network configuration and hyper-parameter settings. The random seed used for training was 42.

Hidden layers	9
Units per hidden layer	256
Hidden layer activation function	Leaky ReLU (neg. slope = 0.3)
λ	0.001
Optimizer	ADAM with default parameters
Initial learning rate	0.001
Learning rate schedule	Divide by 5 every 3 epochs
Training batch size	1024
Validation batch size	8192
Total number of epochs	18
Pre-mask mode	9
Mask mode	9
Number of parameters	
Pre-mask mode	about 0.56 million
Mask mode	about 0.55 million



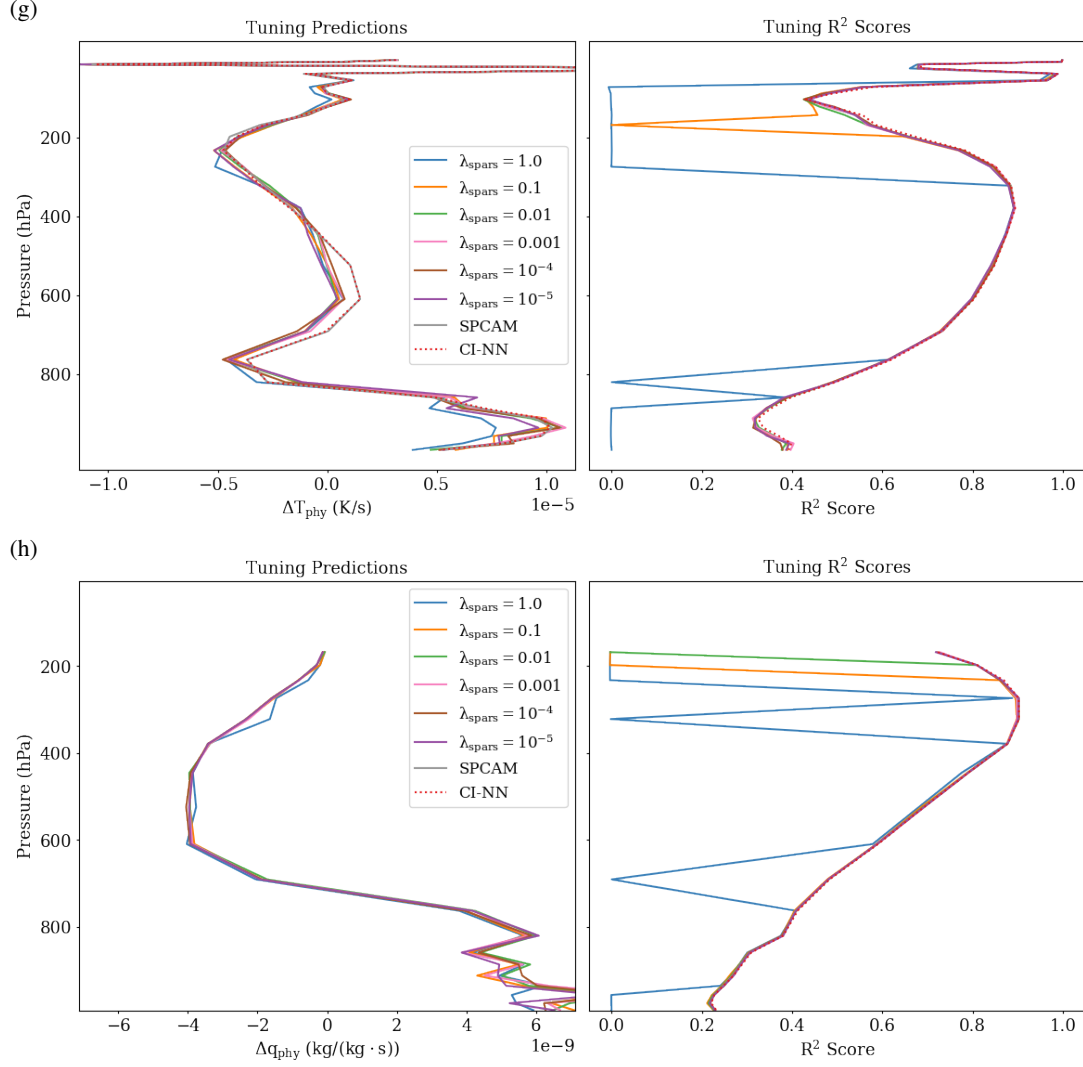


Figure S1: Tuning results for λ in the PCMasking framework exploring a log-spaced search grid $\{1.0, 0.1, \dots, 1 \times 10^{-5}\}$. We find that the neural networks (NNs) trained with $\lambda = 0.001$ give the best performance both in terms of physical consistency (see Fig. S1d) and performance (see Figures S1g and S1h). (a) SHAP values for PCMasking NNs trained with $\lambda = 1.0$. (b) SHAP values for PCMasking NNs trained with $\lambda = 0.1$. (c) SHAP values for PCMasking NNs trained with $\lambda = 0.01$. (d) SHAP values for PCMasking NNs trained with $\lambda = 0.001$. (e) SHAP values for PCMasking NNs trained with $\lambda = 10^{-4}$. (f) SHAP values for PCMasking NNs trained with $\lambda = 10^{-5}$. (g) PCMasking predictions and R^2 scores for temperature tendency ΔT_{phy} for $\lambda \in \{1.0, 0.1, \dots, 1 \times 10^{-5}\}$. (h) PCMasking predictions and R^2 scores for moistening tendency Δq_{phy} for $\lambda \in \{1.0, 0.1, \dots, 1 \times 10^{-5}\}$.

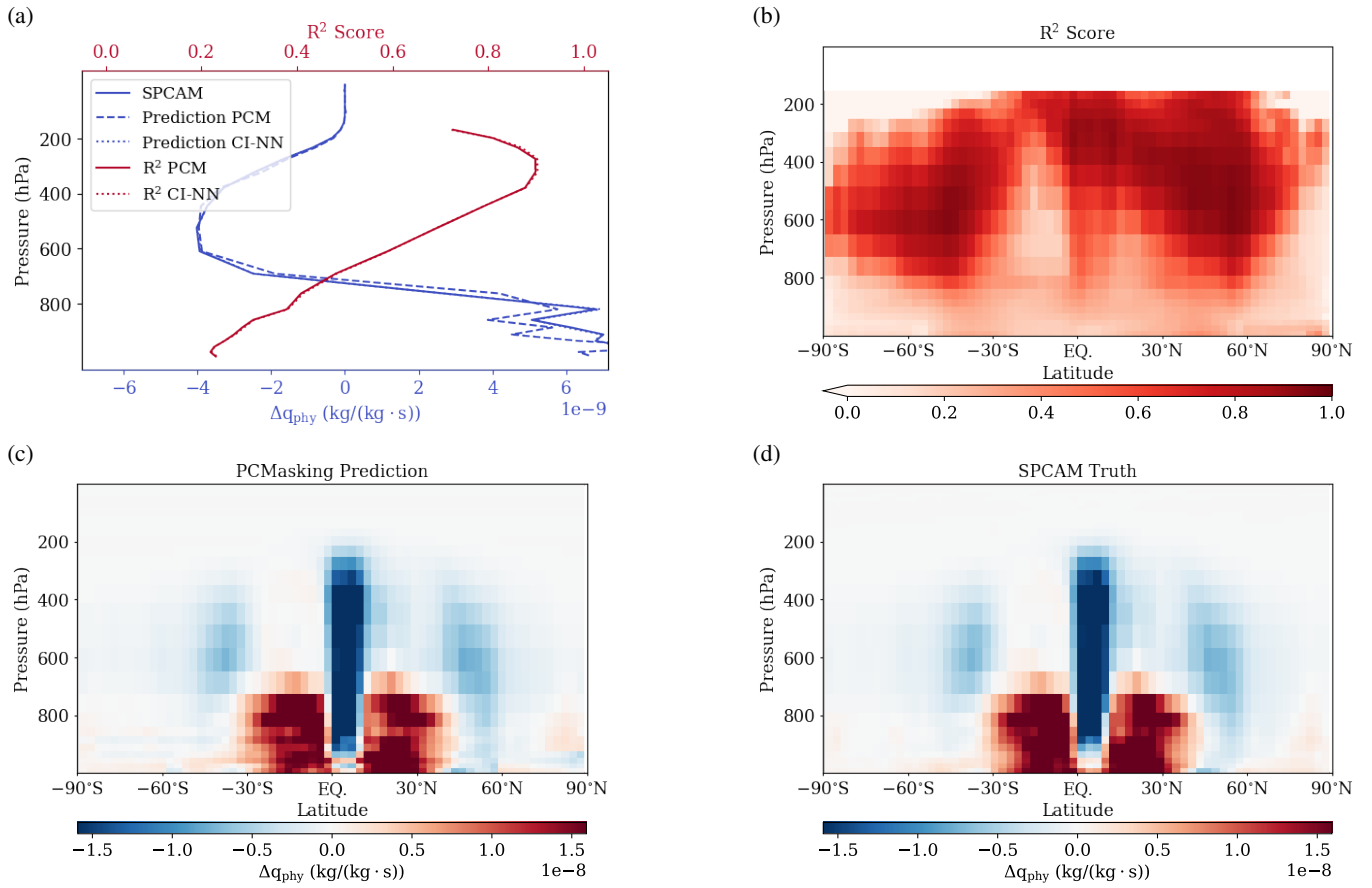


Figure S2: Same as Fig. 2 but for moistening tendency Δq_{phy} . Values are cut off at 168hPa, where we expect negligibly few convective processes due to cold and dry air. PCMasking framework offline evaluation with $\lambda = 0.001$ and thresholds selected based on best training loss performance among 20 thresholds from the interval $[1 \times 10^{-4}, p_{70})$. One network model is trained for each of the 30 vertical levels. All values are averaged for 1440 test data samples. (a) Horizontally averaged vertical profiles for SPCAM truth, prediction and R^2 for causally-informed neural networks (CI-NN) and our PCMasking framework (PCM). (b) Vertical cross-section R^2 for PCMasking framework. (c) Vertical cross-section for PCMasking framework prediction. (d) Vertical cross-section SPCAM truth.

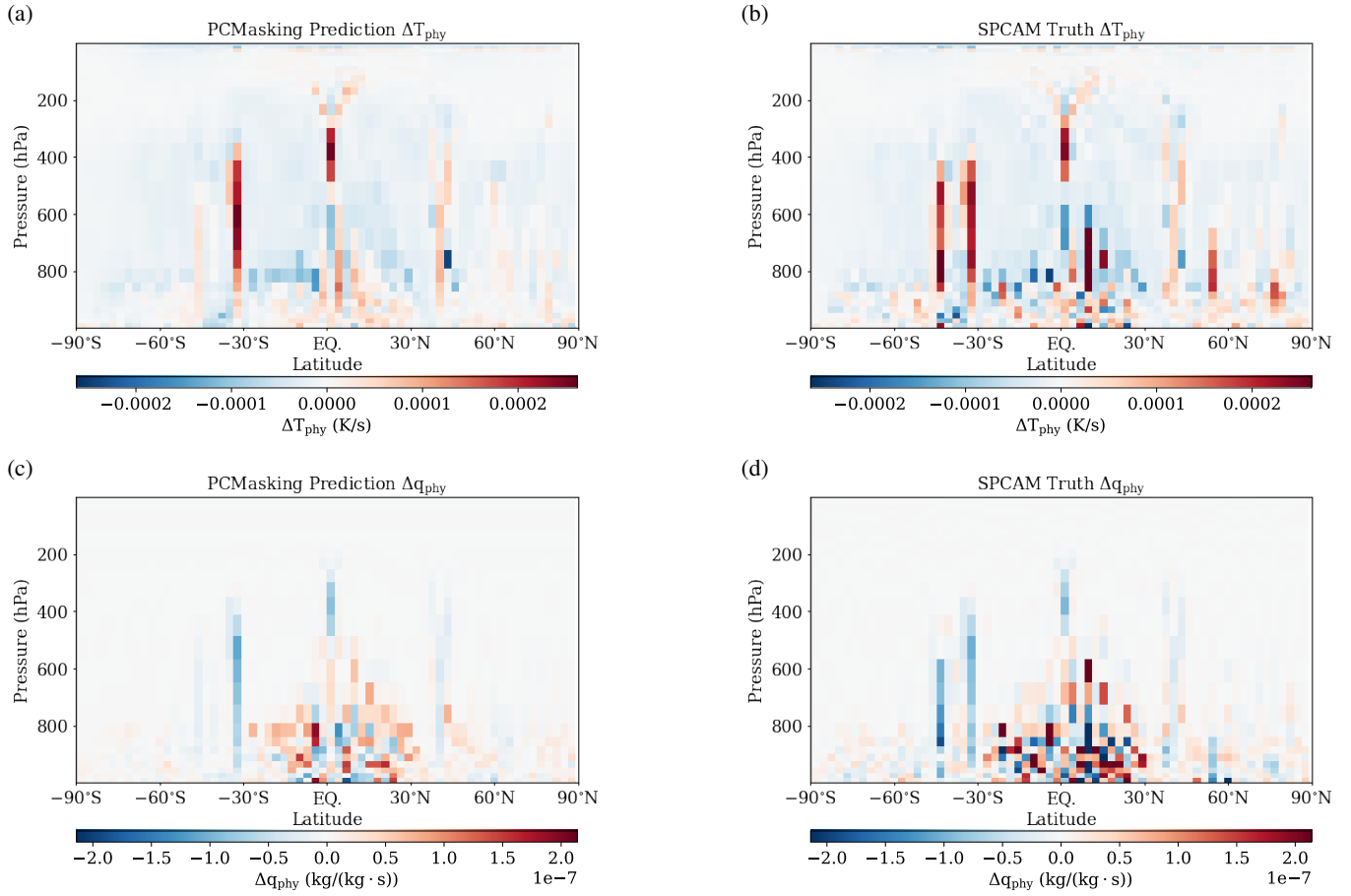


Figure S3: Pressure-latitude cross-section snapshots at time step 500 for PCMasking neural networks (NNs) predictions and SPCAM truth. PCMasking NNs were trained with $\lambda = 0.001$ and thresholds were selected based on best training loss performance among 20 thresholds from the interval $[1 \times 10^{-4}, p_{70})$. One network model is trained for each of the 30 vertical levels. While the predicted and true values show the same general pattern, the NN predictions are considerably smoother and exhibit less extreme values compared to the SPCAM truth. (a) Pressure-latitude cross-section PCMasking NN prediction snapshot at time step 500 for variable temperature tendency ΔT_{phys} . (b) Pressure-latitude cross-section SPCAM truth snapshot at time step 500 for variable temperature tendency ΔT_{phys} . (c) Pressure-latitude cross-section PCMasking NN prediction snapshot at time step 500 for variable moistening tendency Δq_{phys} . (d) Pressure-latitude cross-section SPCAM truth snapshot at time step 500 for variable moistening tendency Δq_{phys} .

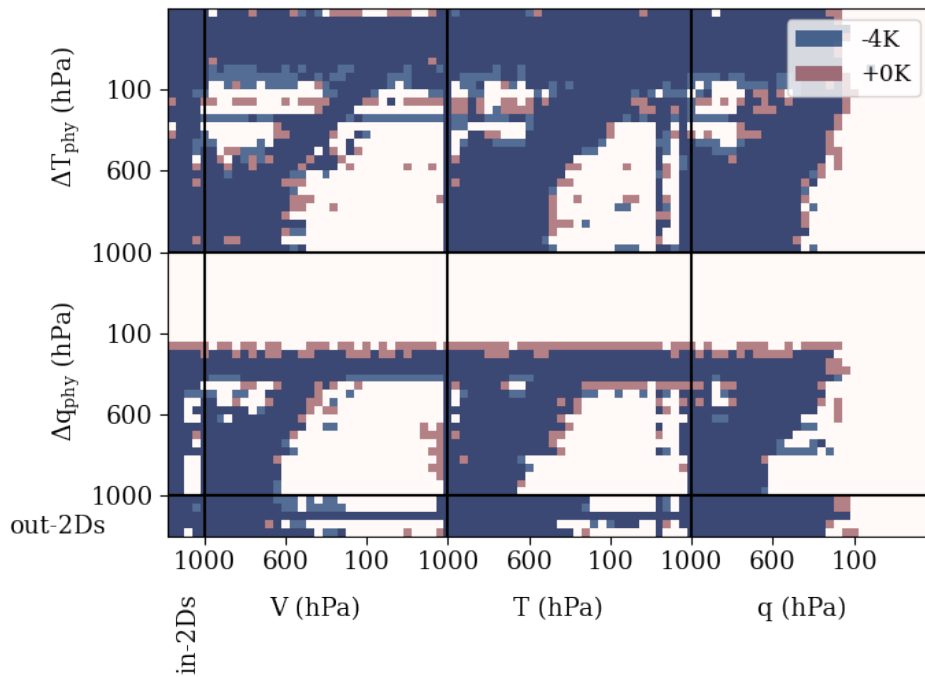


Figure S4: Same as Fig. 4 but for -4K. Comparison of physical driver selection for 0K reference climate and -4K climate in the PCMasking framework. The neural networks were trained with $\lambda = 0.001$ and thresholds were selected based on best training loss performance among 20 thresholds from the interval $[1 \times 10^{-4}, p_{70})$.